Supporting Information

Facile One-Pot Synthesis of Rod-Coil Bio-Block Copolymers and Uncovering Their Role in Forming the Efficient Stretchable Touch-Responsive Light Emitting Diodes

Dai-Hua Jiang,[a,b,c,+] Brian J. Ree,[d,+] Takuya Isono,[d] Xiao-Chao Xia,[d,e] Li-Che Hsu,[b,c] Saburo Kobayashi,[b] Kuan Hoon Ngoi,[f,g] Wei-Cheng Chen,[a] Chih-Chun Jao,[a] Loganathan Veeramuthu,[a] Toshifumi Satoh,[d,] Shih Huang Tung,[c,*] and Chi-Ching Kuo[a,*]*

[a] Institute of Organic and Polymeric Materials, Research and Development Center of Smart Textile Technology, National Taipei University of Technology, 10608 Taipei, Taiwan.

[b] Graduate School of Chemical Sciences and Engineering, Hokkaido University, Sapporo 060-8628, Japan.

[c] Institute of Polymer Science and Engineering, National Taiwan University, 106 Taipei, Taiwan.

[d] Faculty of Engineering, Hokkaido University, Sapporo 060-8628, Japan.

[e] School of Materials Science and Engineering, Chongqing University of Technology, Chongqing 400054, China.

[f] Materials Science Program, Department of Applied Physics, Faculty of Science and Technology, Universiti Kebangsaan Malaysia, Bangi 43600, Selangor, Malaysia.

[g] Department of Chemistry and Pohang Accelerator Laboratory, Pohang University of Science and Technology, Pohang 37673, Republic of Korea.

*Author to whom all correspondence should be addressed

+D. H. J. and B. J. R. contributed equally to this work.

Supplementary Materials

- **Figure S1.** The ^{1}H NMR spectrum of crude aliquots withdrawn from the reaction system for monitoring the conversion of *δ*-DL to form I-PDL.
- **Figure S2.** Polymerization time versus *δ*-DL conversion and Ln($[M]_0/[M]_t$).
- **Figure S3.** The plots of $M_{n,SEC}$ and $Đ$ versus *δ*-DL conversion for indicating a controlled polymerization by TBD.
- **Figure S4.** The ^{1}H NMR spectrum of crude aliquots withdrawn from the reaction system for monitoring the conversion of EGE and the formation of alternative copolymer.
- **Figure S5.** Evolution of SEC traces after Suzuki–Miyaura catalyst transfer polymerization (SCTP) (a) PF_{18}-*b*-(PA-*alt*-EGE)$_{20}$ and (b) PF_{18}-*b*-(AA-*alt*-EGE)$_{20}$.
- **Figure S6.** The ^{1}H NMR spectrum of the resultant PF_{18}-*b*-(PA-*alt*-EGE)$_{20}$ via smart synthesis isolated from the mixture by precipitation in cold toluene.
- **Figure S7.** The ^{1}H NMR spectrum of the resultant PF_{18}-*b*-(AA-*alt*-EGE)$_{20}$ via smart synthesis isolated from the mixture by precipitation in cold toluene.
- **Figure S8.** The ^{1}H NMR spectrum of the resultant PF_{18}-*b*-PDL_{13} via smart synthesis isolated from the mixture by precipitation in cold acetone (in $CDCl_3$).
- **Figure S9.** The ^{1}H NMR spectrum of the resultant PF_{18}-*b*-PDL_{24} via smart synthesis isolated from the mixture by precipitation in cold acetone (in $CDCl_3$).
- **Figure S10.** The ^{1}H NMR spectrum of the resultant PF_{18}-*b*-PDL_{36} via smart synthesis isolated from the mixture by precipitation in cold acetone (in $CDCl_3$).
- **Figure S11.** The ^{13}C NMR with peak designation of the polymerization of PF_{18}-*b*-PDL_{36} via smart synthesis (in $CDCl_3$).
- **Figure S12.** Representative COSY NMR spectrum of PF_{18}-*b*-PDL_{36} in $CDCl_3$.
- **Figure S13.** Representative HMQC NMR spectrum of PF_{18}-*b*-PDL_{36} in $CDCl_3$.
- **Figure S14.** DOSY NMR spectrum of the polymer blend of PF_{18} and PDL_{36} in $CDCl_3$.
- **Figure S15.** TGA thermograms of studied polymers measured with a temperature ramping rate of 10 °C min^{-1} under nitrogen atmosphere.

- **Figure S16.** 2nd heating DSC thermograms of studied polymers measured with a temperature ramping rate of 10 °C min^{-1} under nitrogen atmosphere.
- **Figure S17.** Synchrotron GIWAXS data of thin films of block copolymers measured with SDD = 208.3 mm at room temperature using a synchrotron X-ray beam (λ = 0.12359 nm).
- **Figure S18.** AFM phase images of the thin films of block copolymers.
- **Figure S19.** AFM height images of the thin films of block copolymers.
- **Figure S20.** PL emission spectra of the as-cast and annealed film of block copolymers.
- **Figure S21.** Correlation between integrated PL intensity and temperature derived from (a) PF_{18} (b) PF_{18}-*b*-PDL_{13} (c) PF_{18}-*b*-PDL_{24} (d) PF_{18}-*b*-PDL_{36}, where exciton binding energy is extracted by fitting the curve.
- **Figure S22.** Energy levels of the studied materials.
- **Figure S23.** Voltage dependent luminance and current properties of block copolymers.
- **Figure S24.** OM images of the studied polymers of as-cast film at the strain of 0%, 50%, 100%, 150% and 200%.
- **Figure S25.** Photographs of LED device at strains of 0%, 50%, 100%, 150%, and 200% respectively.
- **Figure S26.** Luminance-stretching cycle characteristics of the touch-responsive LEDs after repetitive stretching cycles at (a) 20% and (b) 40% strain.
- **Table S1.** Smart synthesis of conjugated block copolymer under organcatalysts using difuncational initiator.
- **Table S2.** Smart synthesis of PF-based conjugated block copolymer under TBD using difunctional initiator.
- **Table S3.** Thermal properties of studied polymers.
- **Table S4.** Optical properties of studied polymers.
- **Table S5.** The time-resolved PL spectra of PF_{18}-*b*-PDL_n thin films of as-cast state.

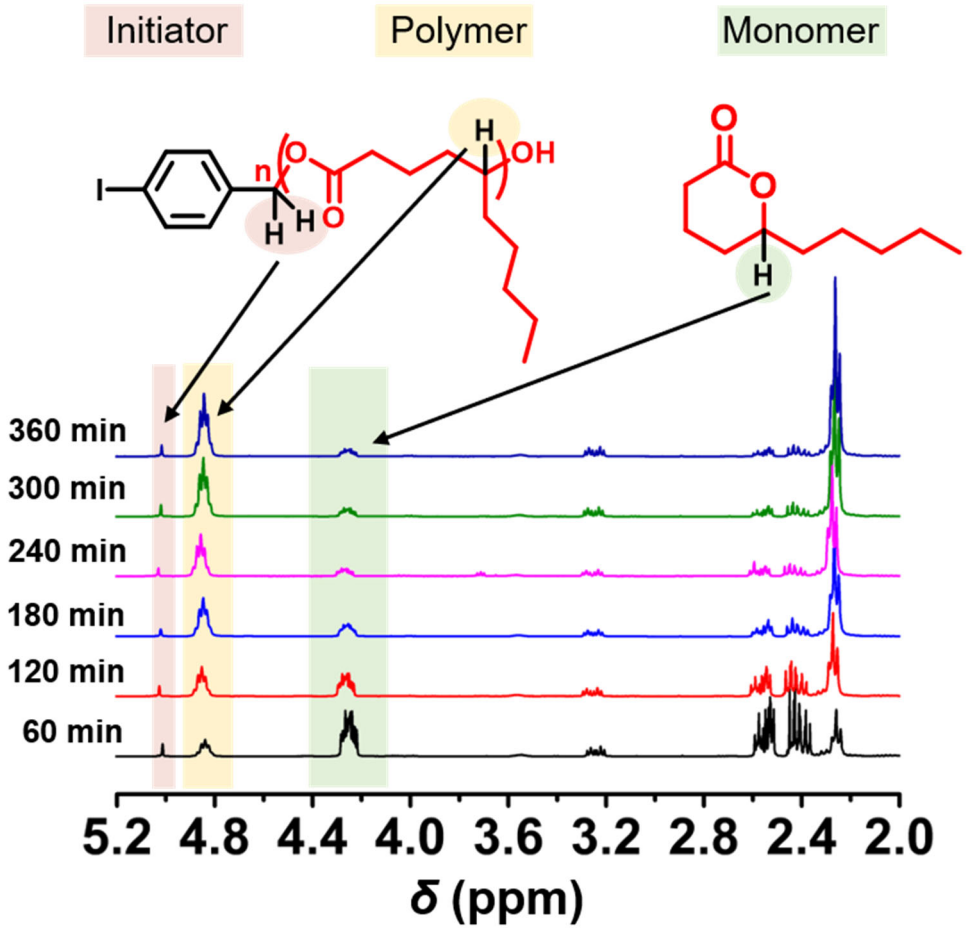

Figure S1. The ^{1}H NMR spectrum of crude aliquots withdrawn from the reaction system for monitoring the conversion of δ-DL to form I-PDL (The ROP is conducted in bulk at 25°C, [TBD]:[4-iodobenzyl alcohol]:[δ-DL] = 1 : 1 : 60).

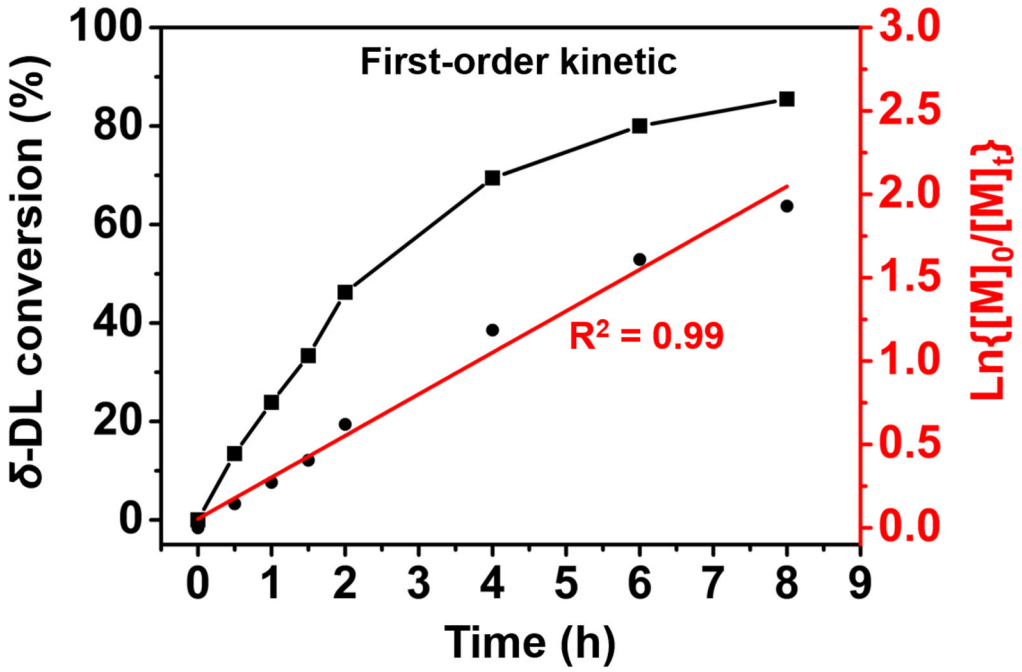

Figure S2. Polymerization time versus δ-DL conversion and Ln($[M]_0/[M]_t$) (The polymerization is conducted in bulk at 25°C, [TBD]:[4-iodobenzyl alcohol]$_0$:[δ-DL]$_0$ = 1 : 1 : 60).

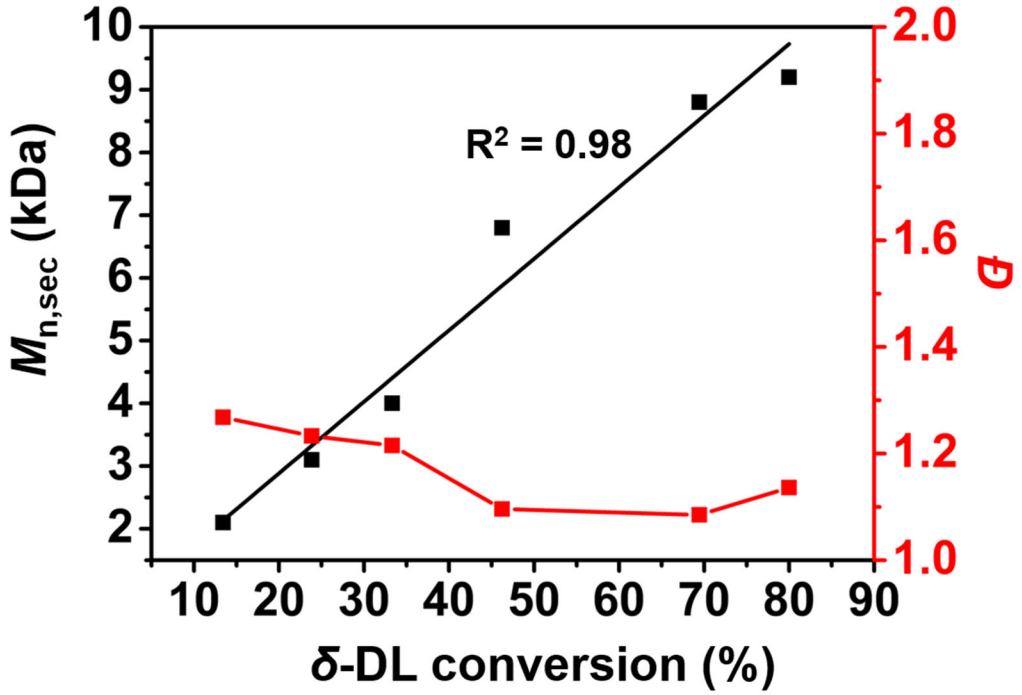

Figure S3. The plots of $M_{n,SEC}$ and $Đ$ versus δ-DL conversion for indicating a controlled polymerization by TBD (The polymerization is conducted in bulk at 25°C, [TBD]:[4-iodobenzyl alcohol]$_0$:[δ-DL]$_0$ = 1 : 1 : 60).

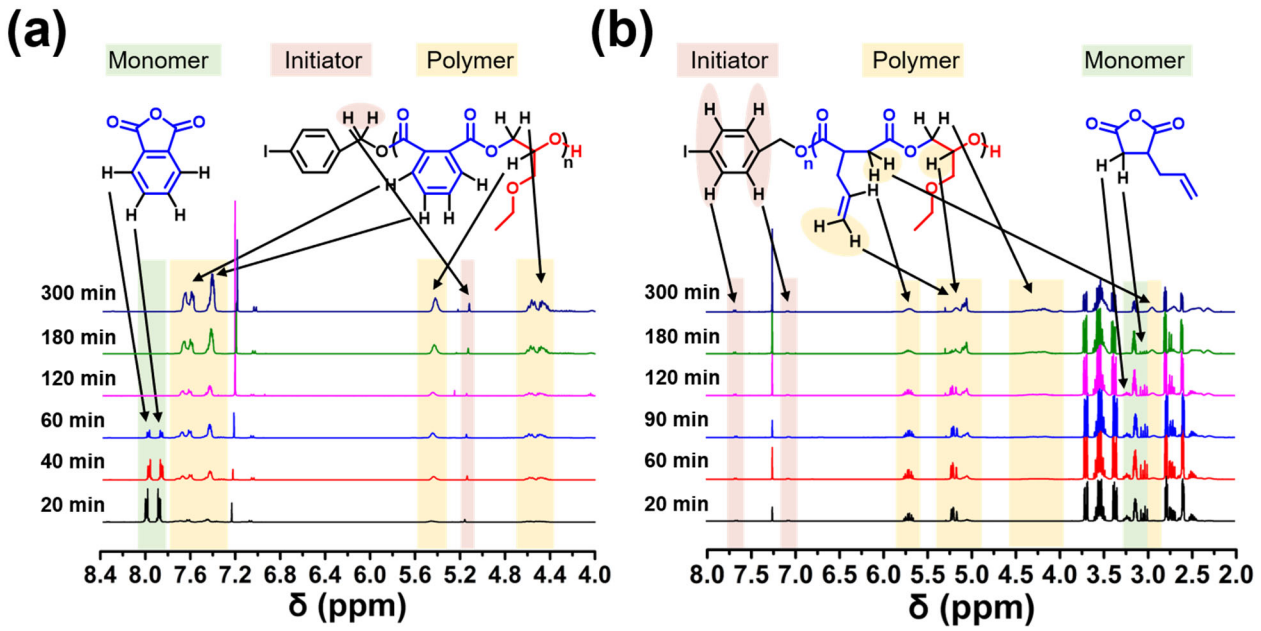

Figure S4. The 1H NMR spectrum of crude aliquots withdrawn from the reaction system for monitoring the conversion of EGE and the formation of alternative copolymer (a) PA-*alt*-EGE and (b) AA-*alt*-EGE.

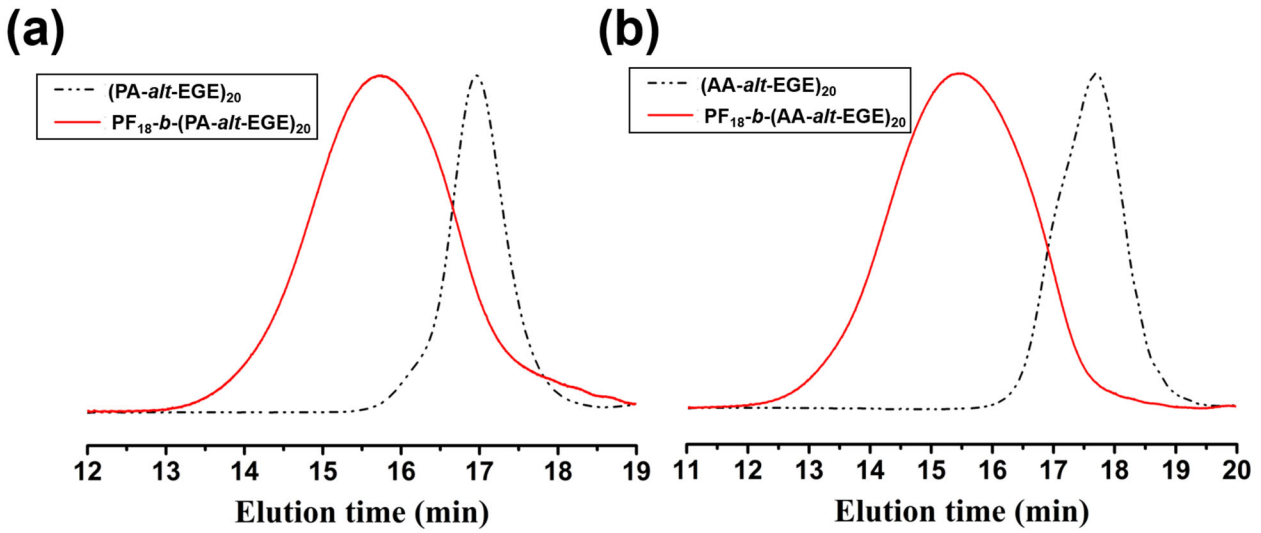

Figure S5. Evolution of SEC traces after Suzuki–Miyaura catalyst transfer polymerization (SCTP) (a) PF_{18}-*b*-(PA-*alt*-EGE)$_{20}$ and (b) PF_{18}-*b*-(AA-*alt*-EGE)$_{20}$.

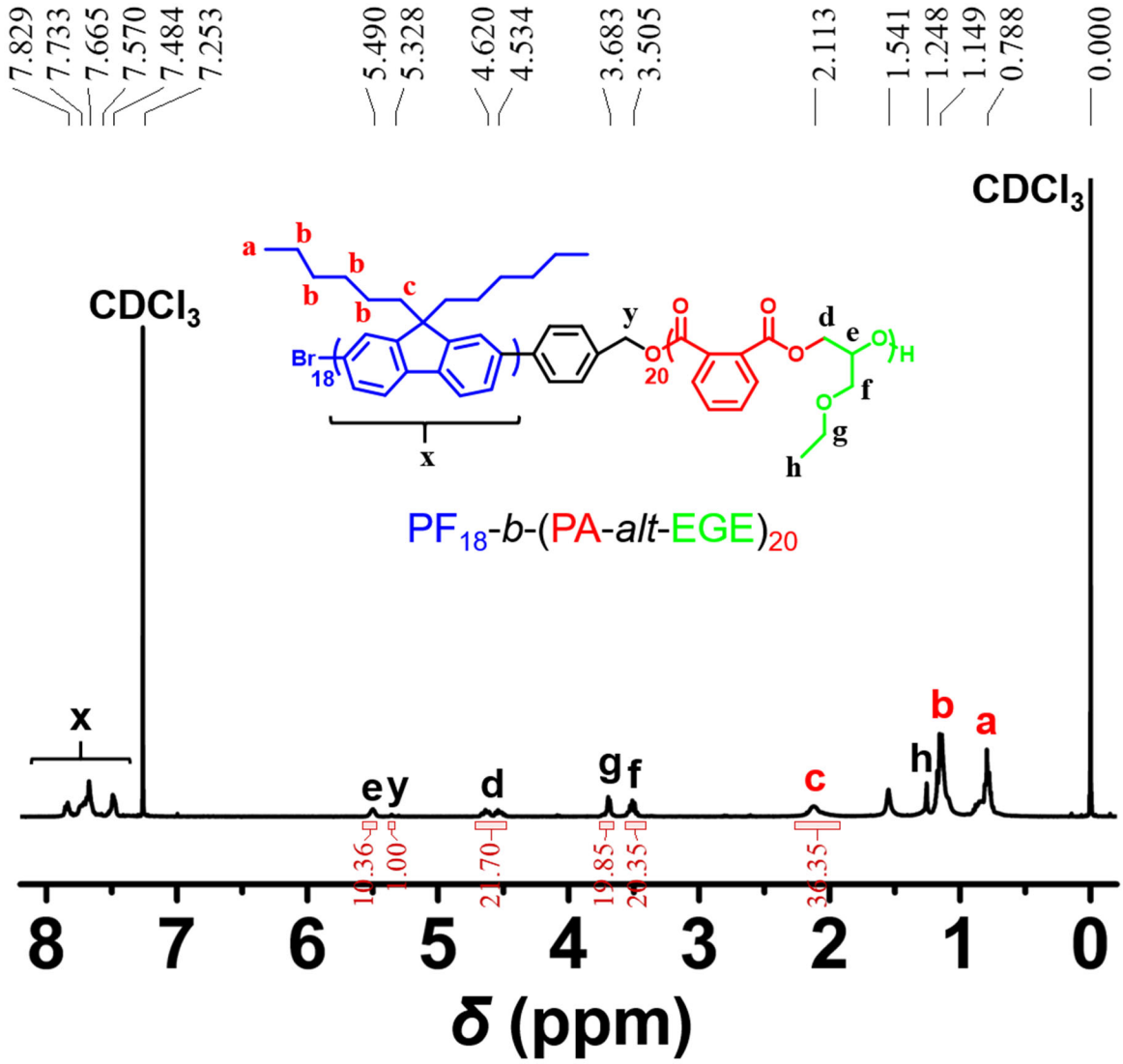

Figure S6. The ^{1}H NMR spectrum of the resultant PF_{18}-*b*-(PA-*alt*-EGE)$_{20}$ via smart synthesis isolated from the mixture by precipitation in cold toluene.

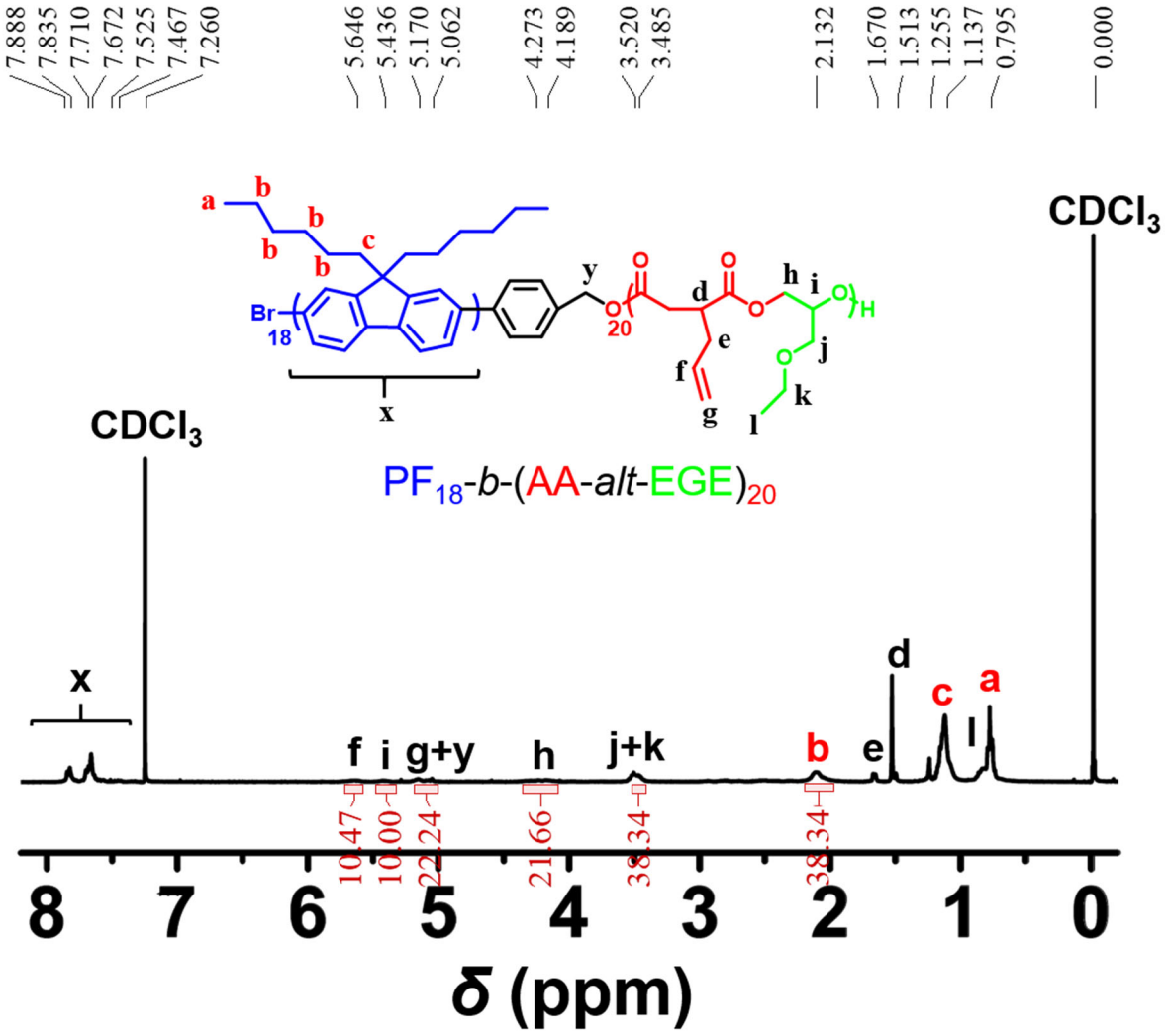

Figure S7. The ^{1}H NMR spectrum of the resultant PF_{18}-*b*-(AA-*alt*-EGE)$_{20}$ via smart synthesis isolated from the mixture by precipitation in cold toluene.

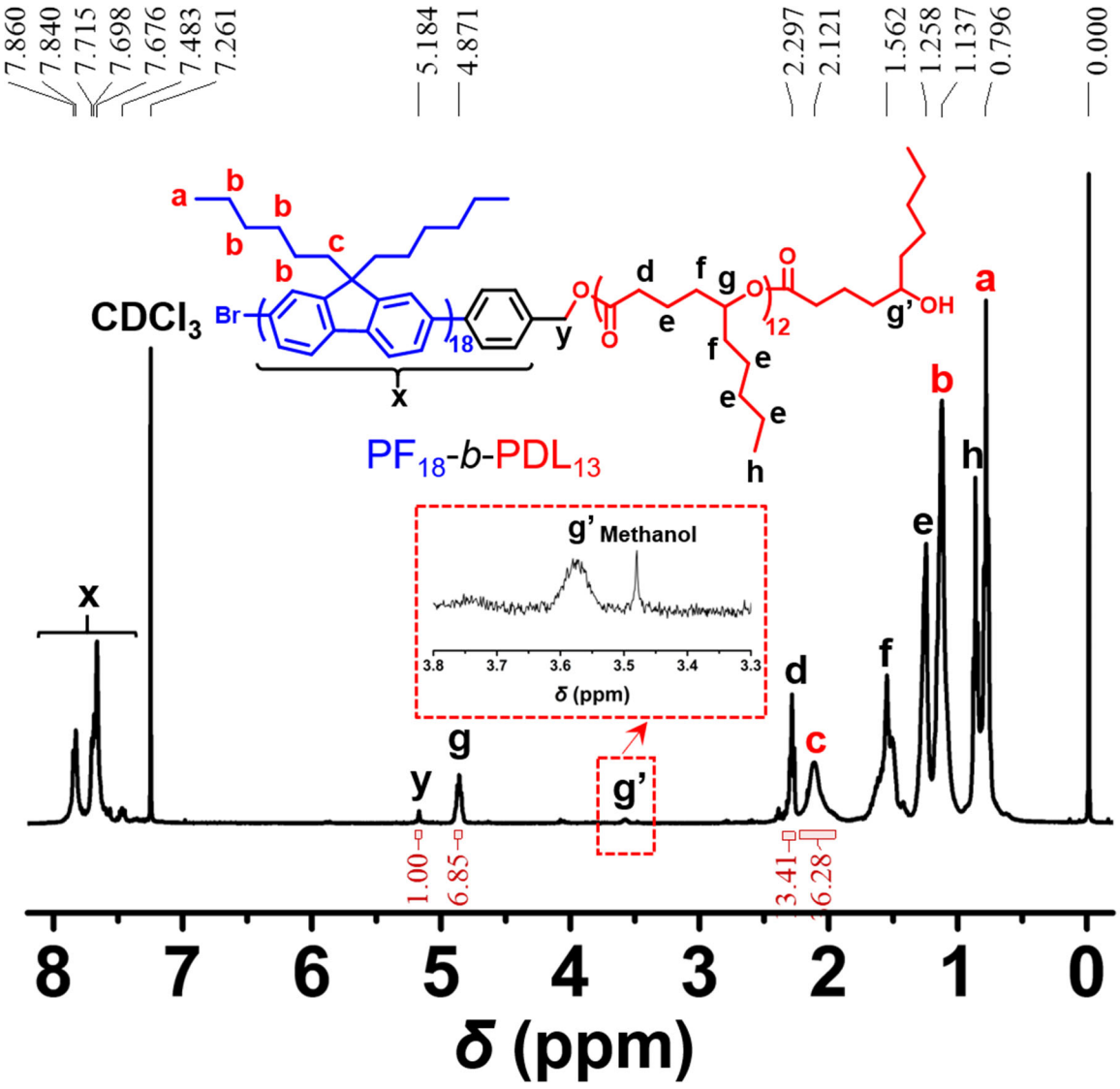

Figure S8. The ^{1}H NMR spectrum of the resultant PF_{18}-*b*-PDL_{13} via smart synthesis isolated from the mixture by precipitation in cold acetone (in $CDCl_3$).

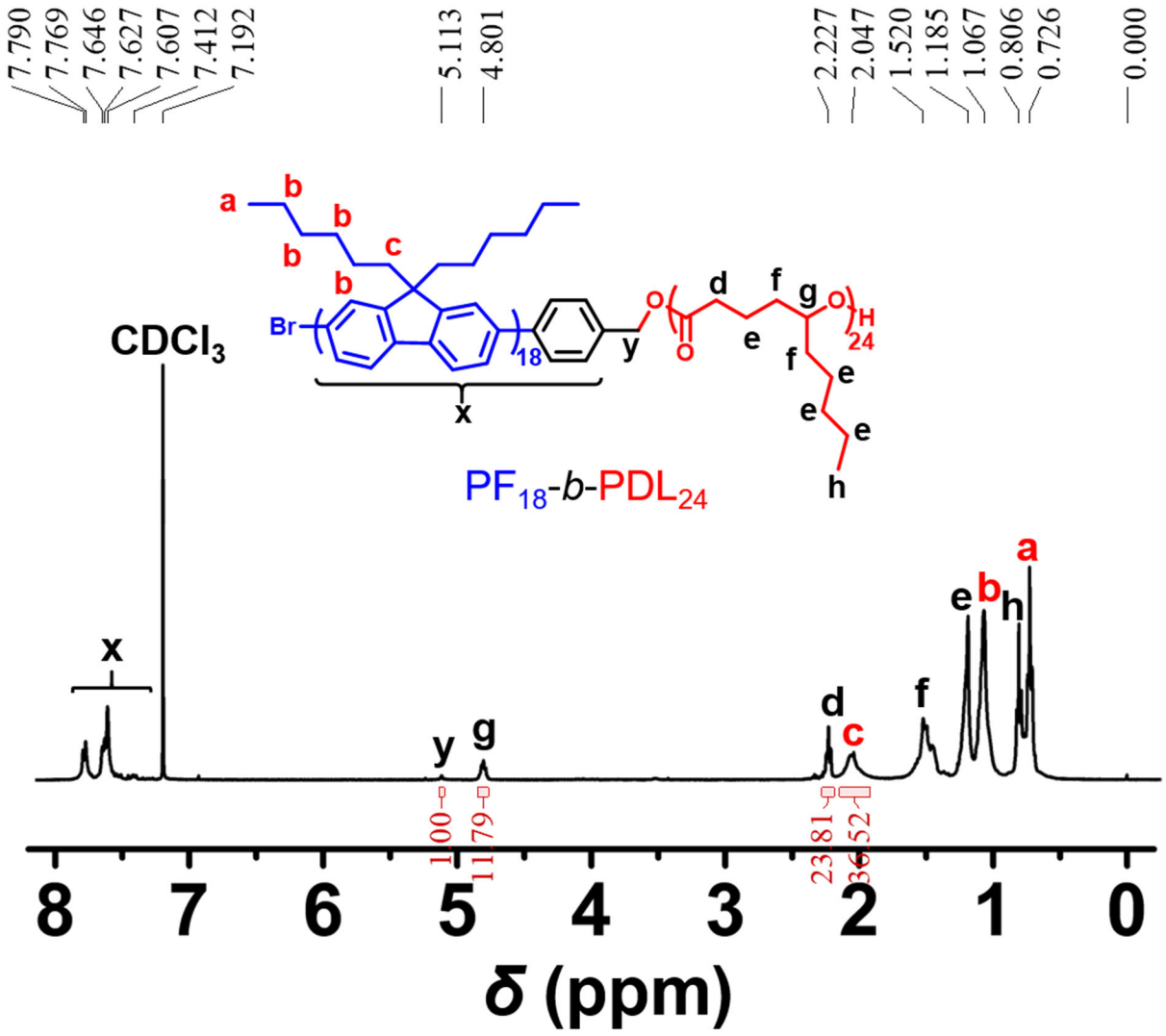

Figure S9. The ^{1}H NMR spectrum of the resultant PF_{18}-*b*-PDL_{24} via smart synthesis isolated from the mixture by precipitation in cold acetone (in $CDCl_3$).

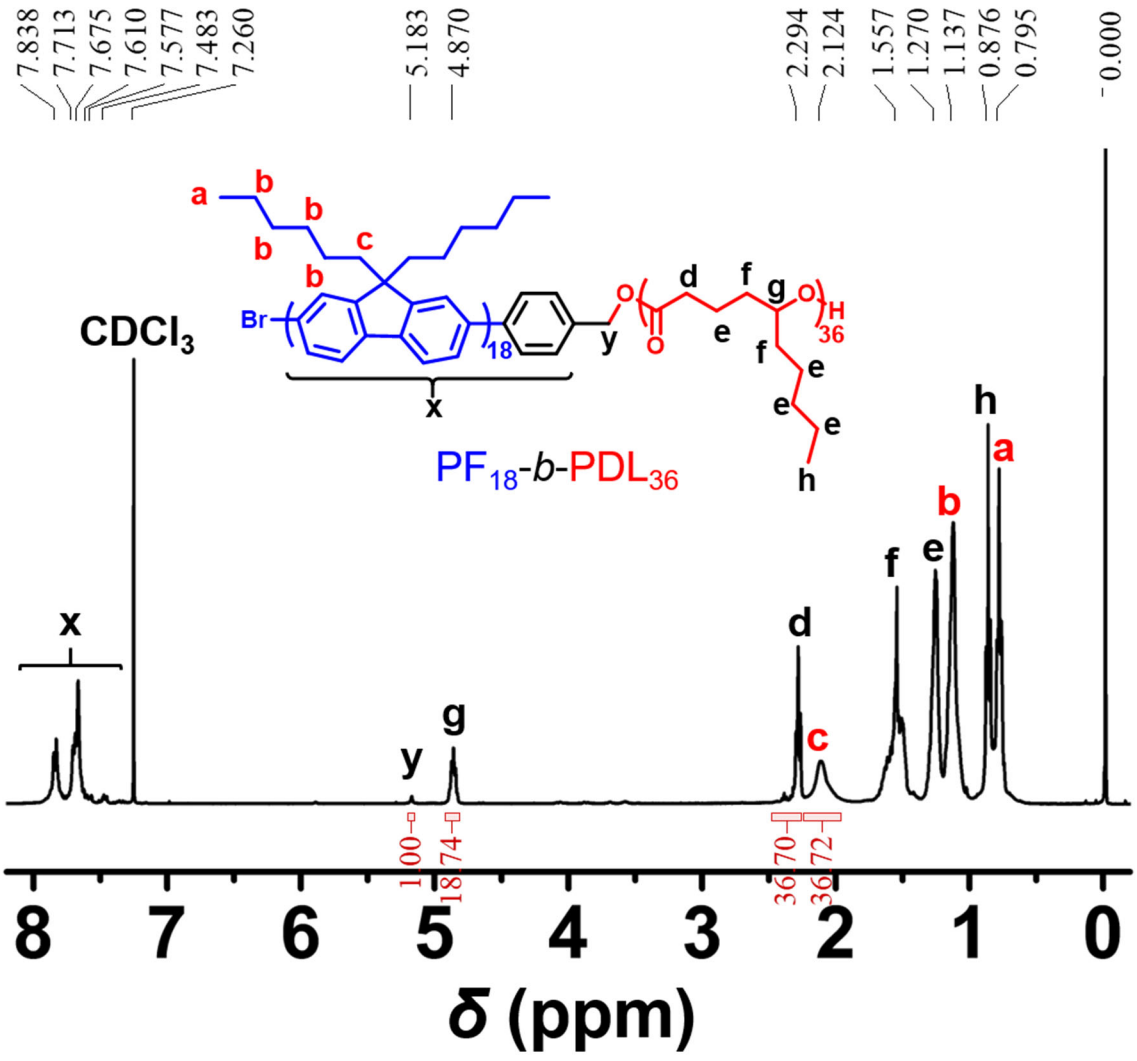

Figure S10. The ^{1}H NMR spectrum of the resultant PF_{18}-*b*-PDL_{36} via smart synthesis isolated from the mixture by precipitation in cold acetone (in $CDCl_3$).

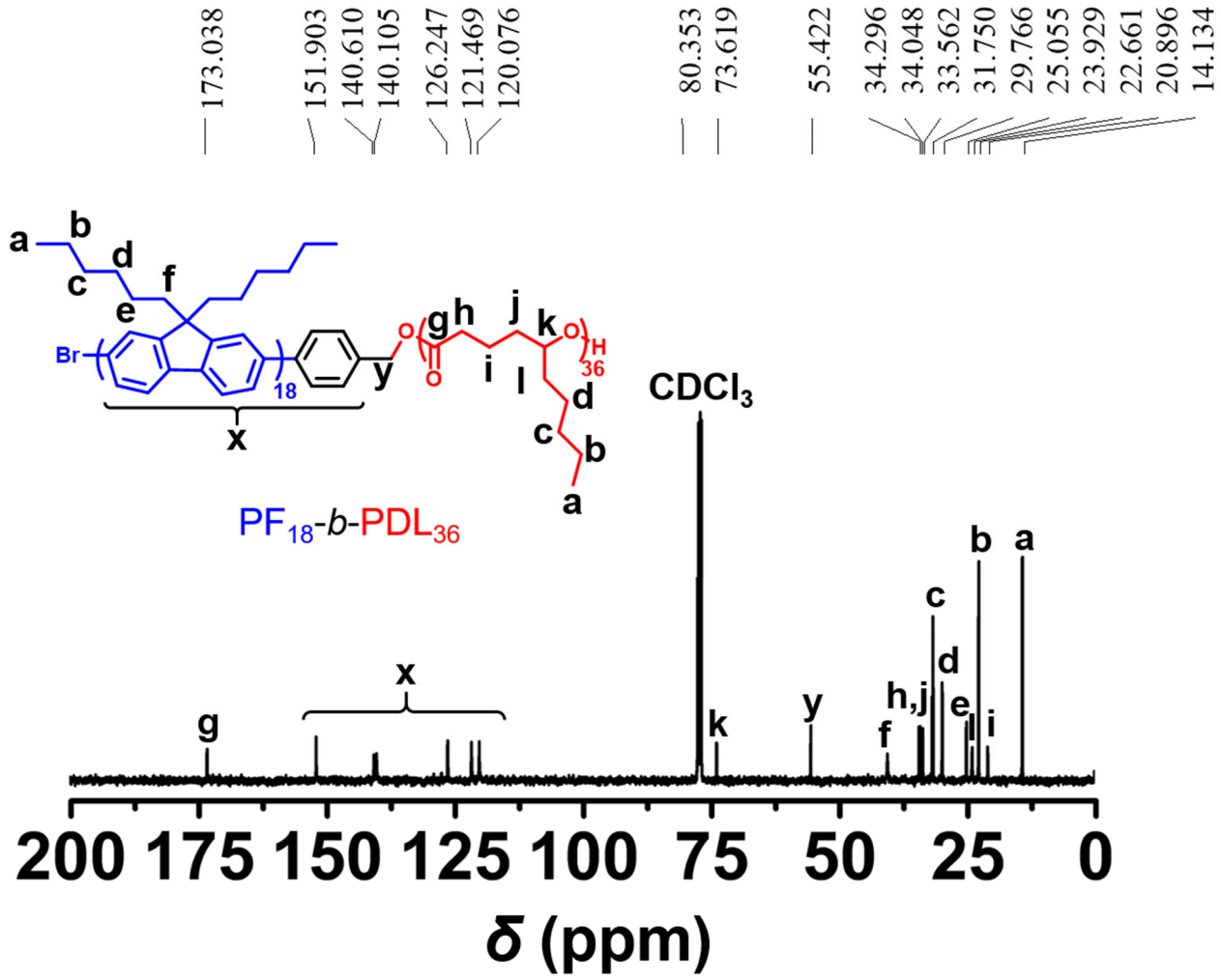

Figure 11. The ^{13}C NMR with peak designation of the polymerization of PF_{18}-*b*-PDL_{36} via smart synthesis (in $CDCl_3$).

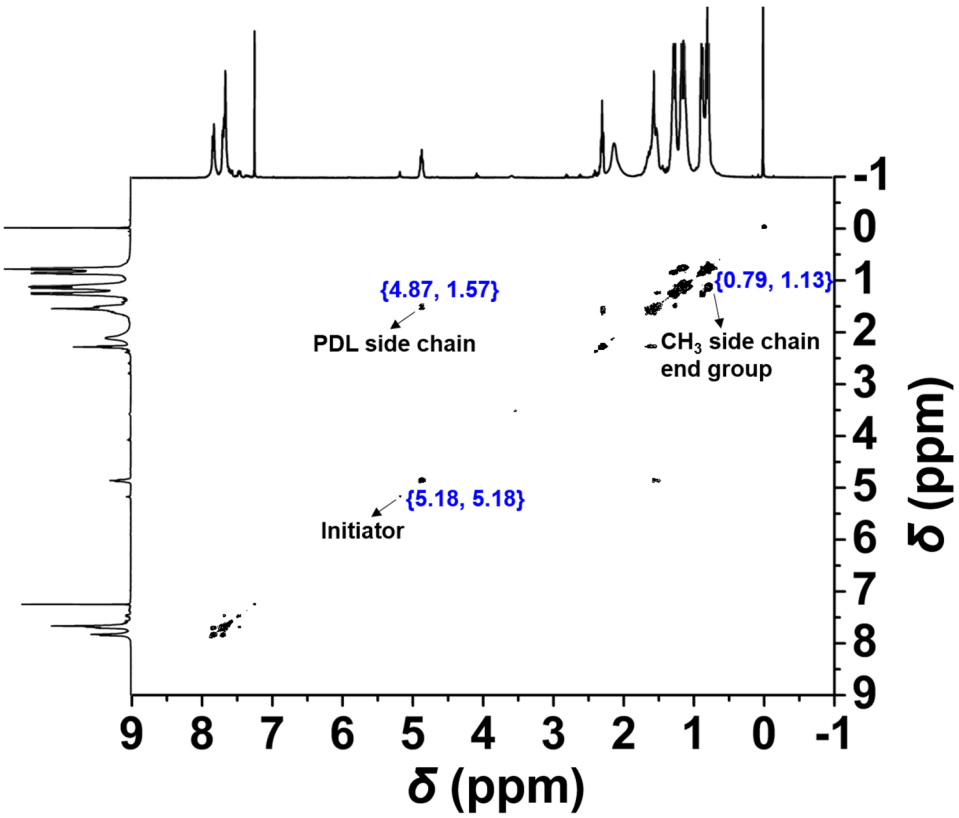

Figure S12. Representative COSY NMR spectrum of PF_{18}-*b*-PDL_{36} in $CDCl_3$.

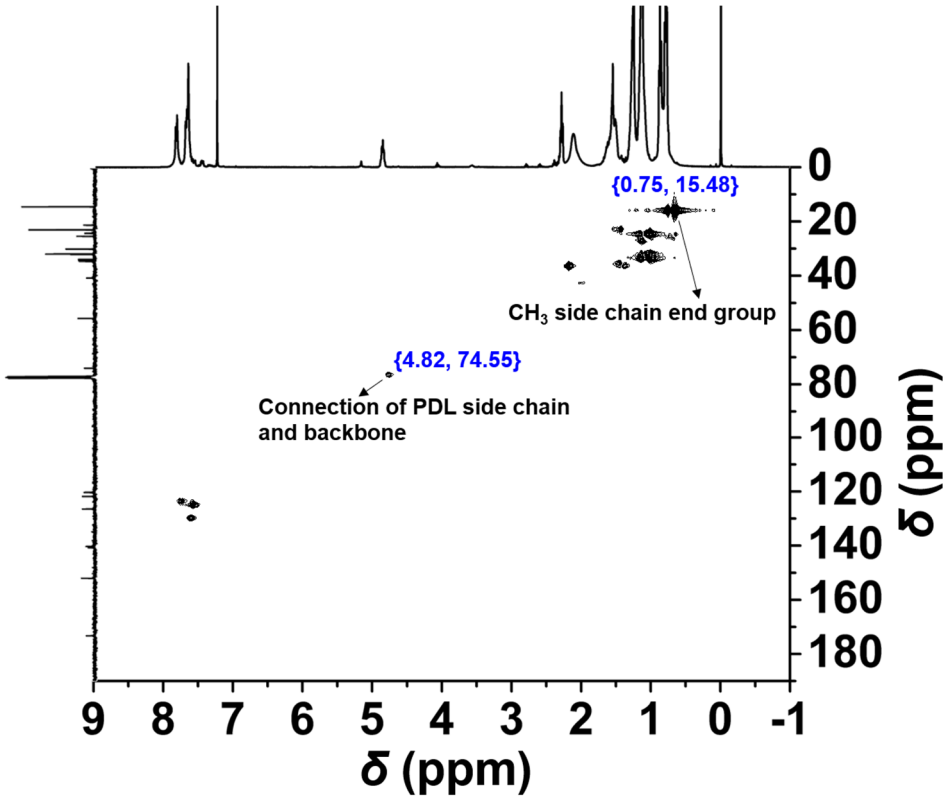

Figure S13. Representative HMQC NMR spectrum of PF_{18}-*b*-PDL_{36} in $CDCl_3$.

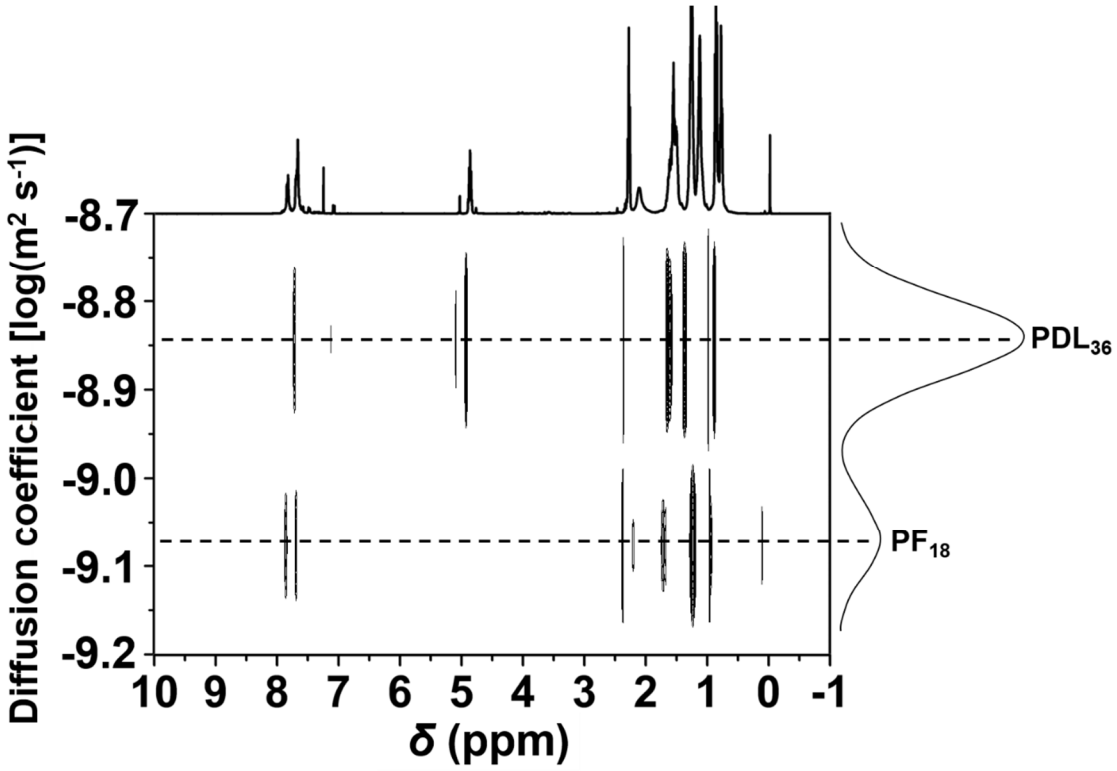

Figure S14. DOSY NMR spectrum of the polymer blend of PF_{18} and PDL_{36} in $CDCl_3$.

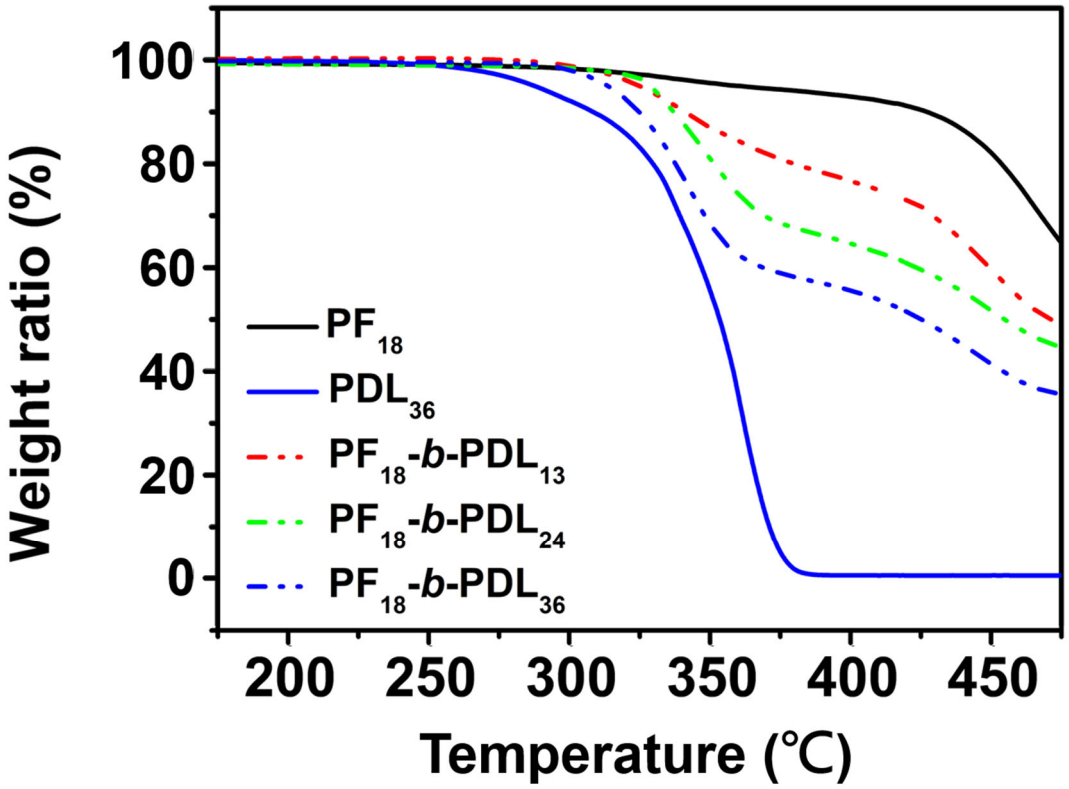

Figure S15. TGA curves of studied polymers measured with a temperature ramping rate of 10 °C min^{-1} under nitrogen atmosphere.

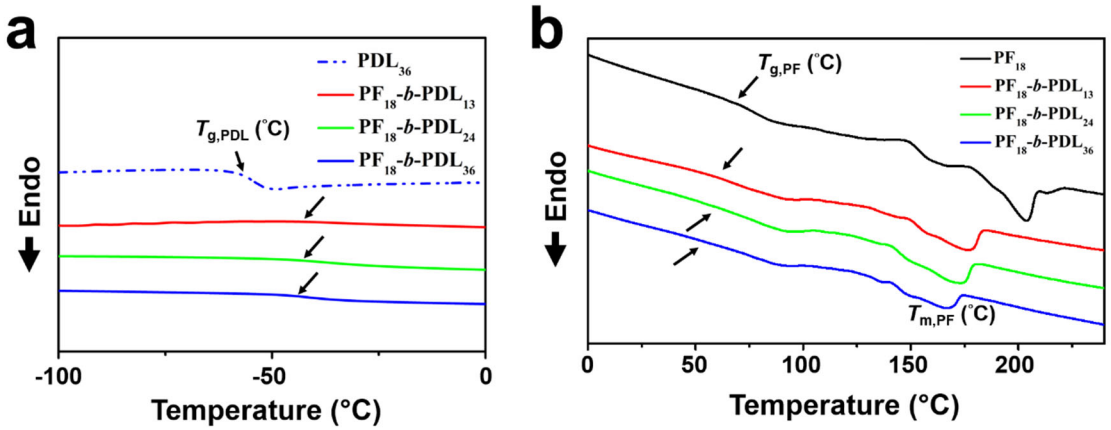

Figure S16. 2nd heating DSC thermograms of studied polymers measured with a temperature ramping rate of 10 °C min^{-1} under nitrogen atmosphere. The arrow from a and b show the expanded DSC curves for highlighting the T_g from PDL and PF block, respectively.

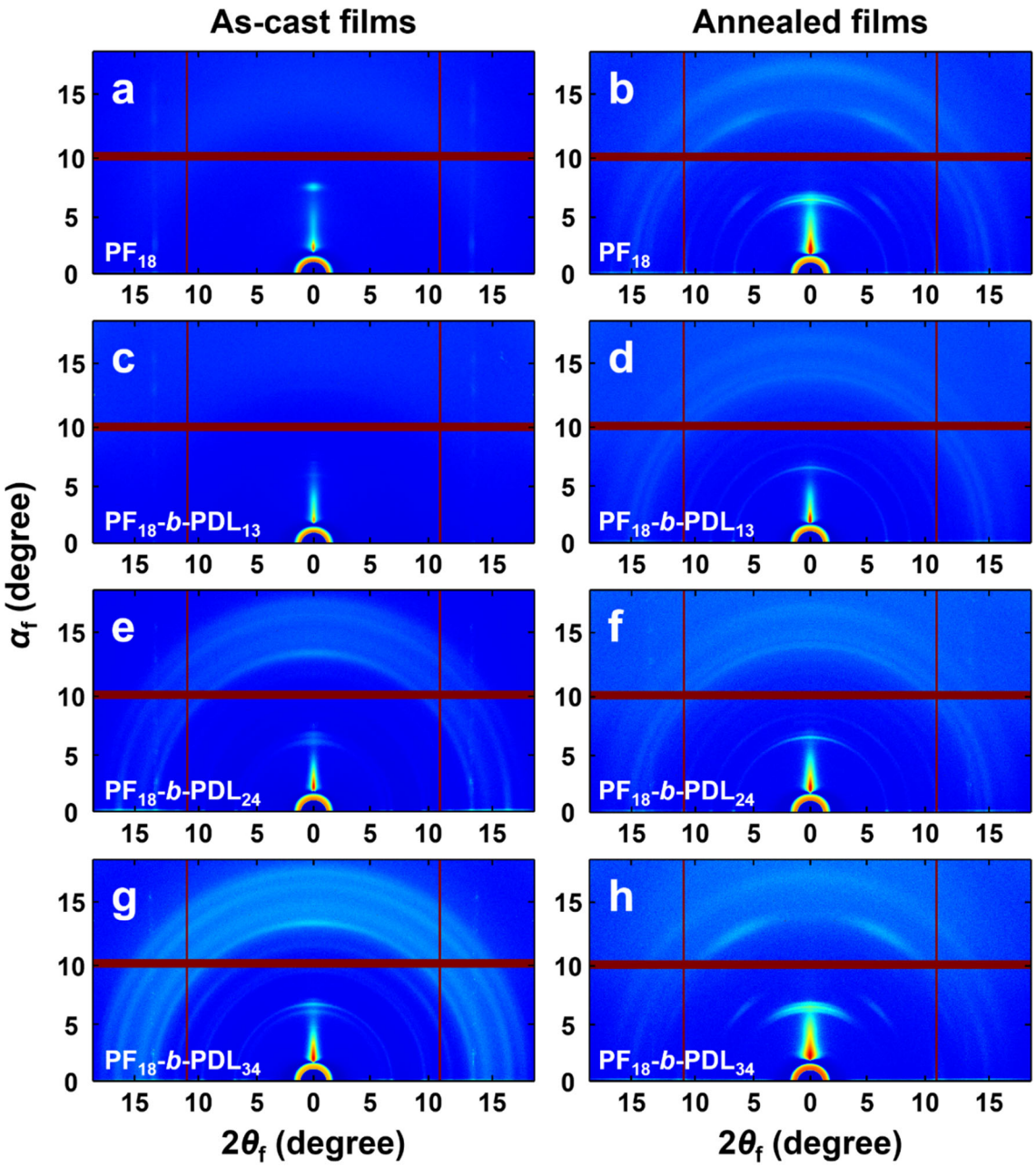

Figure S17. Synchrotron GIWAXS data of thin films of block copolymers measured with SDD = 208.3 mm at room temperature using a synchrotron X-ray beam (λ = 0.12359 nm). (a) PF_{18} as-cast film (α_i = 0.144°). (b) PF_{18} annealed film (α_i = 0.155°). (c) PF_{18}-*b*-PDL_{13} as-cast film (α_i = 0.196°). (d) PF_{18}-*b*-PDL_{13} annealed film (α_i = 0.155°). (e) PF_{18}-*b*-PDL_{24} as-cast film (α_i = 0.134°). (f) PF_{18}-*b*-PDL_{24} annealed film (α_i = 0.155°). (g) PF_{18}-*b*-PDL_{36} as-cast film (α_i = 0.093). h) PF_{18}-*b*-PDL_{36} annealed film (α_i = 0.165°).

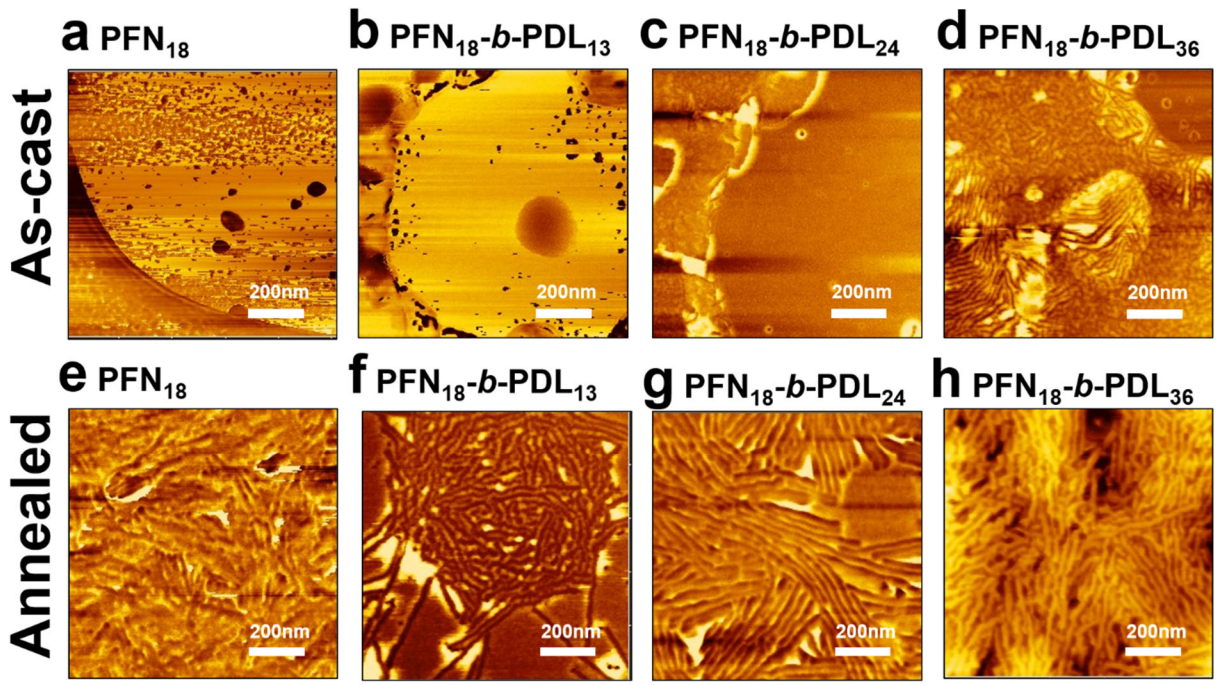

Figure S18. AFM phase images of the thin films of block copolymers. (a) PF_{18} as-cast film. (b) PF_{18}-*b*-PDL_{13} as-cast film. (c) PF_{18}-*b*-PDL_{24} as-cast film. (d) PF_{18}-*b*-PDL_{36} as-cast film. (e) PF_{18} annealed film. (f) PF_{18}-*b*-PDL_{13} annealed film. (g) PF_{18}-*b*-PDL_{24} annealed film. (h) PF_{18}-*b*-PDL_{36} annealed film.

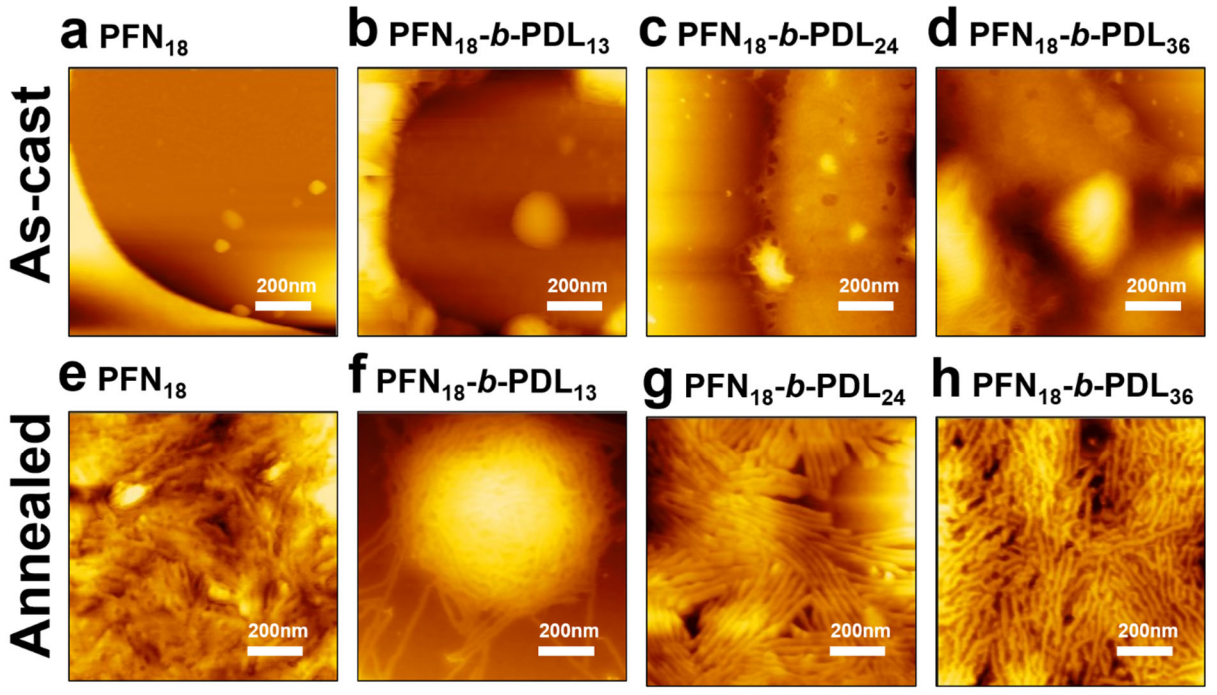

Figure S19. AFM height images of the thin films of block copolymers. (a) PF_{18} as-cast film. (b) PF_{18}-*b*-PDL_{13} as-cast film. (c) PF_{18}-*b*-PDL_{24} as-cast film. (d) PF_{18}-*b*-PDL_{36} as-cast film. (e) PF_{18} annealed film. (f) PF_{18}-*b*-PDL_{13} annealed film. (g) PF_{18}-*b*-PDL_{24} annealed film. (h) PF_{18}-*b*-PDL_{36} annealed film.

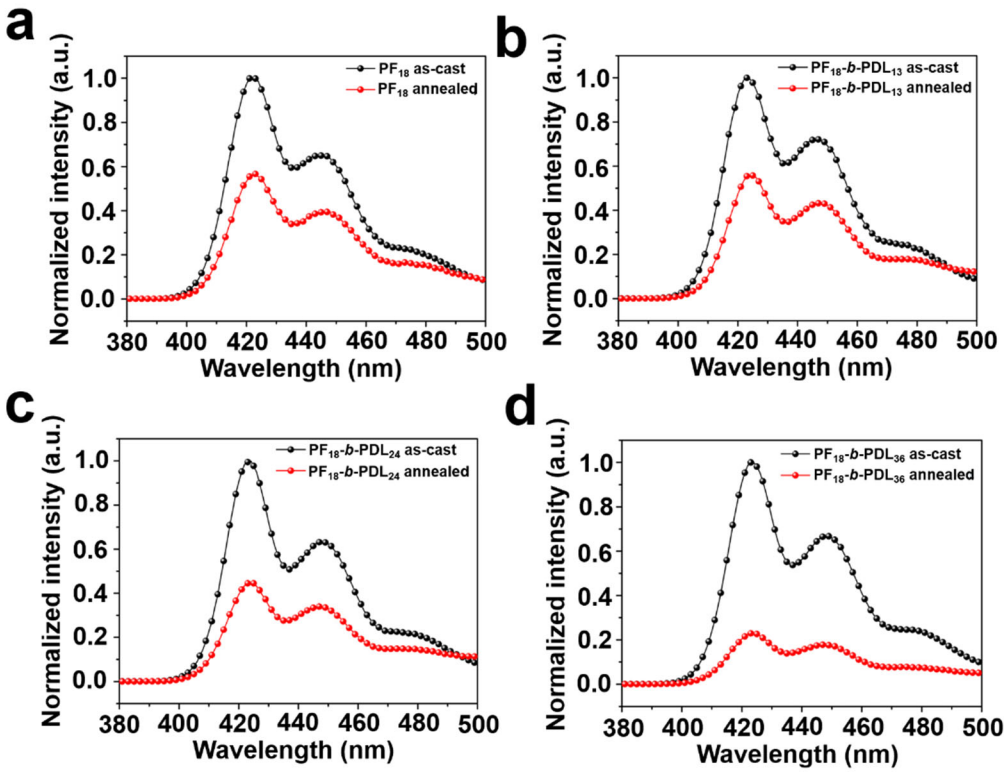

Figure S20. PL emission spectra of the as-cast and annealed film of block copolymers. (a) PF_{18}. (b) PF_{18}-*b*-PDL_{13}. (c) PF_{18}-*b*-PDL_{24}. (d) PF_{18}-*b*-PDL_{36}.

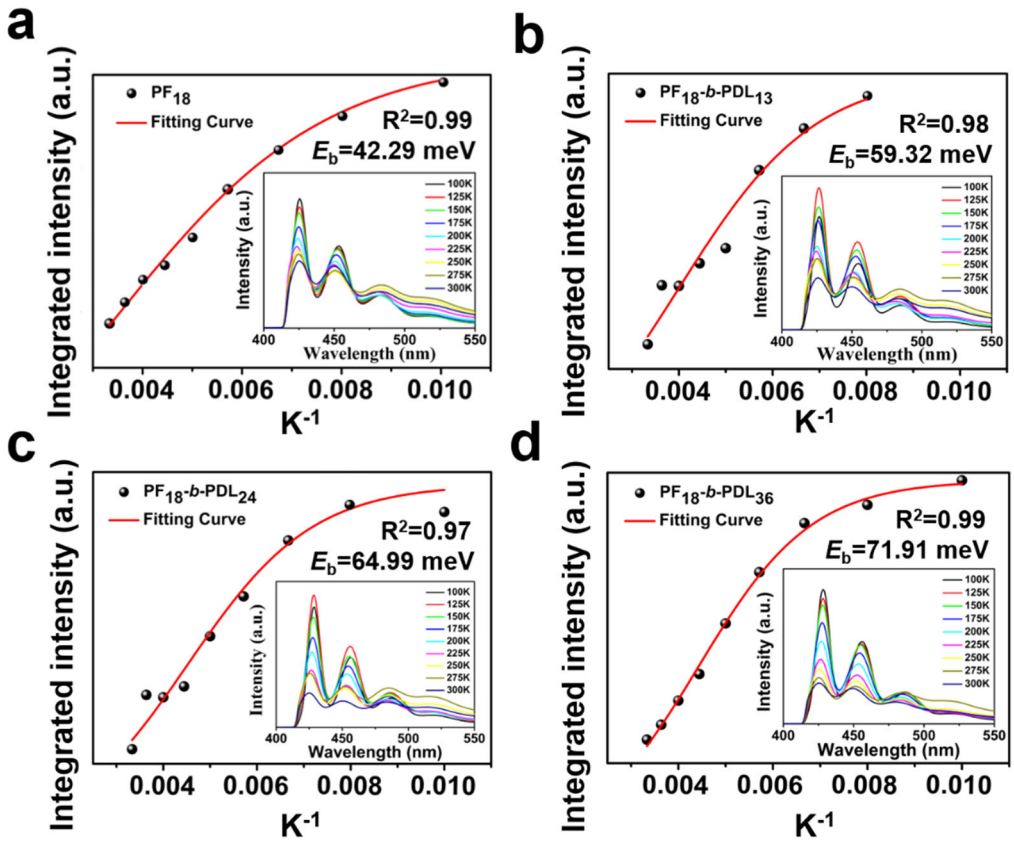

Figure S21. Correlation between integrated PL intensity and temperature. (a) PF_{18}. (b) PF_{18}-*b*-PDL_{13}. (c) PF_{18}-*b*-PDL_{24}. (d) PF_{18}-*b*-PDL_{36}. Exciton binding energy is extracted by fitting the curve.

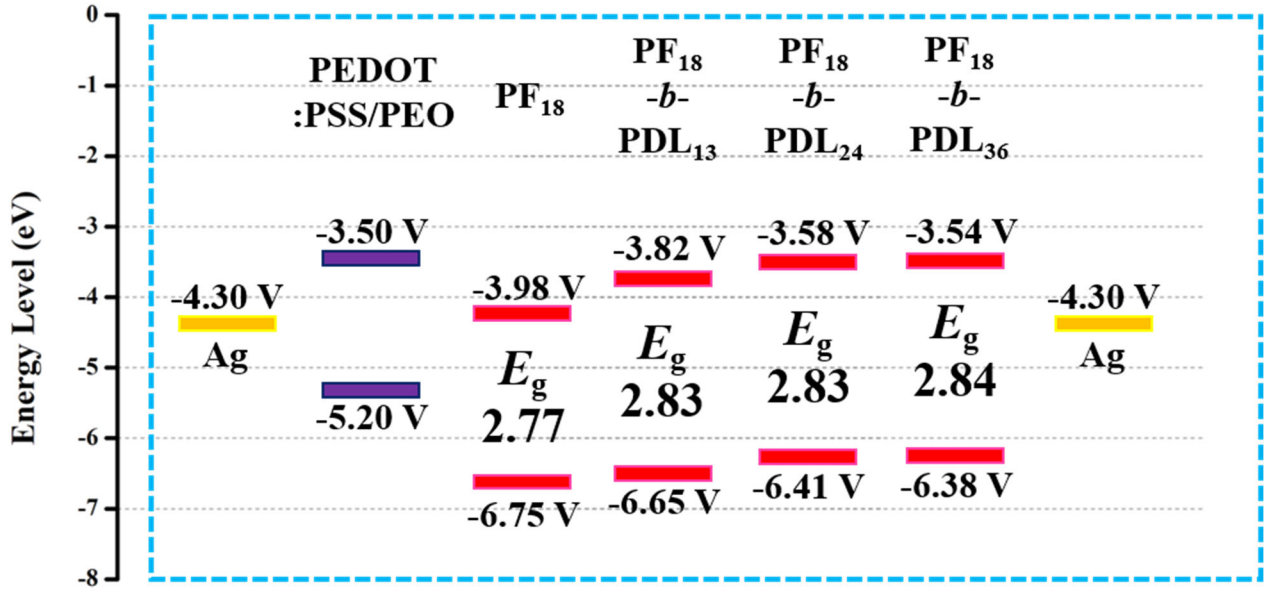

Figure S22. Energy levels of the studied materials.

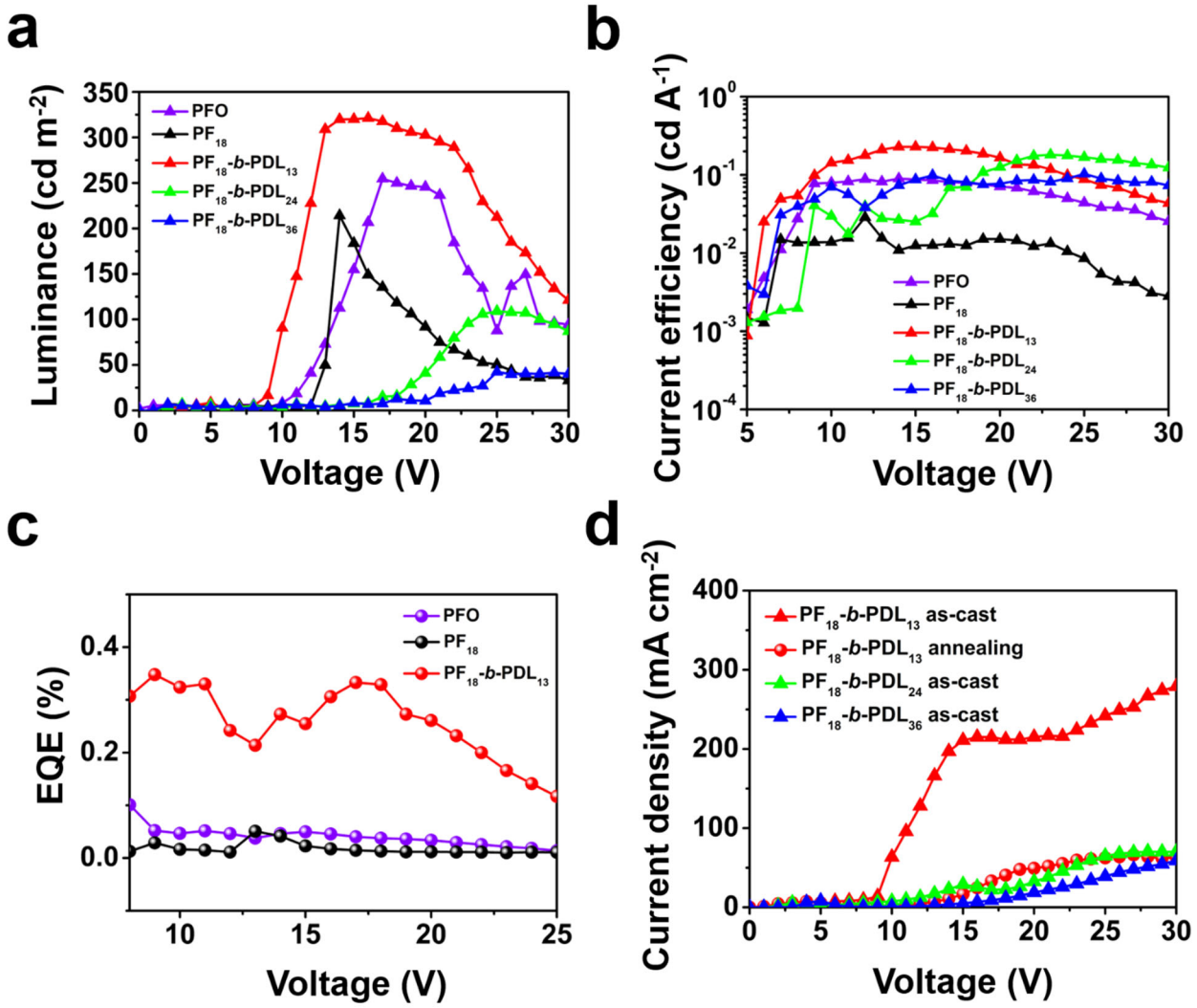

Figure S23. Voltage dependent luminance and current properties of block copolymers. (a) luminace-voltage plot characteristics of as-cast thin films of studied polymers. (b) current efficiency-voltage characteristics of as-cast thin films of studied polymers. (c) external quantum efficiency-voltage characteristics of annealed thin films of PFO, PF_{18}, and PF_{18}-*b*-PDL_{13}. (d) current density-voltage characteristics of PF_{18}-*b*-PDL_n block copolymers.

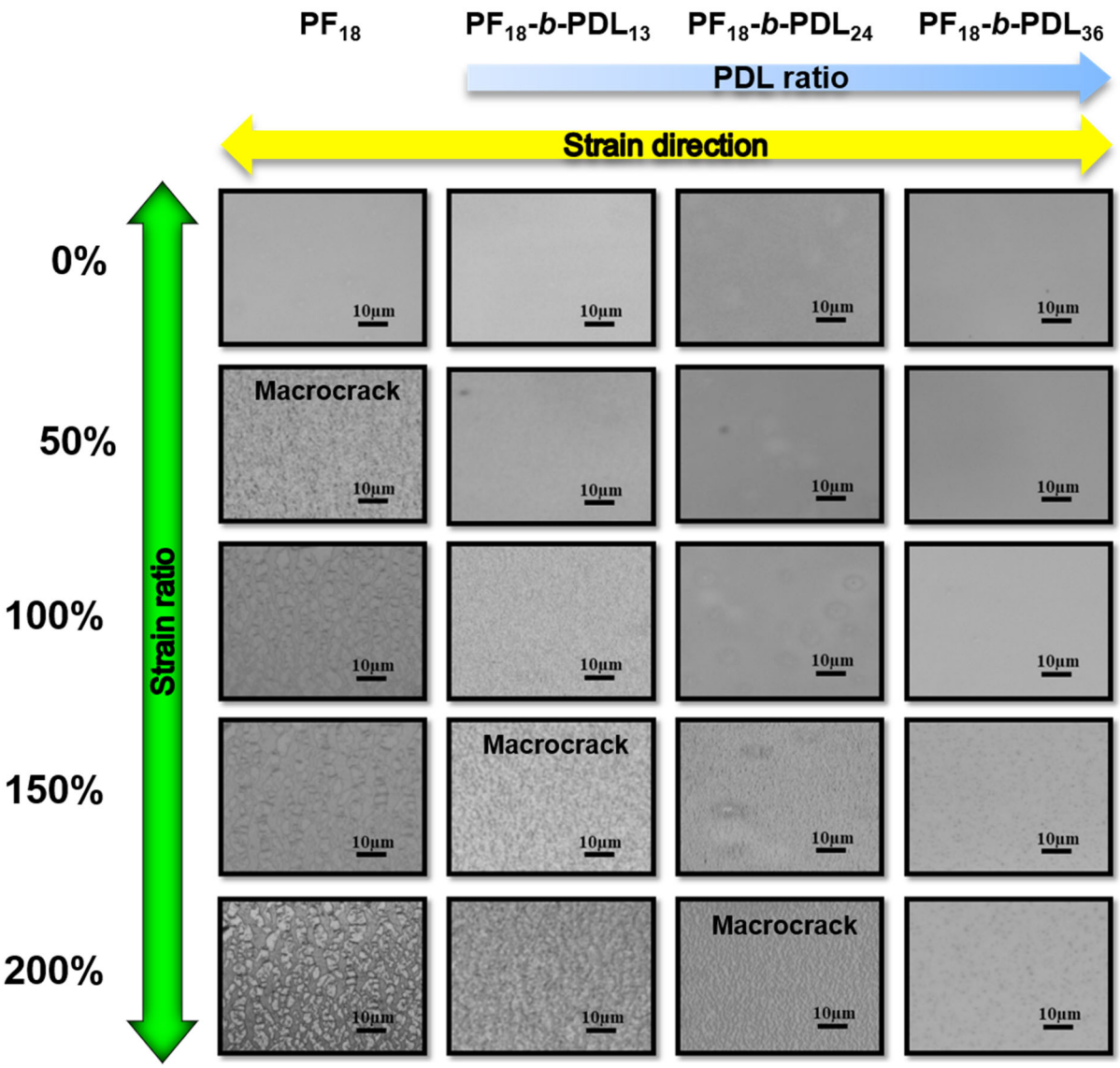

Figure S24. OM images of the studied polymers of as-cast film at the strain of 0%, 50%, 100%, 150% and 200%.

Figure S25. Photographs of LED device at strains of 0, 50, 100, 150%, and 200% respectively. (a) PF_{18} (b) PF_{18}-*b*-PDL_{13}.

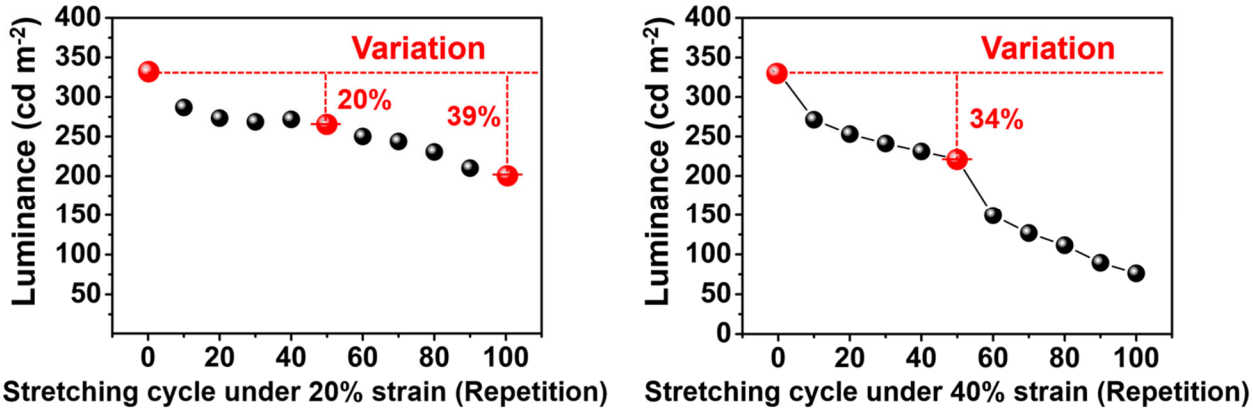

Figure S26. Luminance-stretching cycle characteristics of the touch-responsive LEDs after repetitive stretching cycles at (a) 20% and (b) 40% strain.

Table S1. Smart synthesis of PF-based conjugated block copolymer under TBD using difunctional initiator.

Run	Sample	$[M]_{ROP}$: $[M]_{HexFL}$: $[Initiator]_0$: $[TBD]_{ROP}$	Time (min)	T (°C) [ROP, SCP]	Conv. (%) (ROP)	Conv. (%) (HexFL)	$M_{n,NMR}$ [b] (g mol^{-1})	$M_{n,SEC}$ [c] (g mol^{-1})	$Đ$ [c]	Yield (%)
1	PF_{18}	0:18:1:0	10	-10	-	>99	6,300	11,000	1.327	82.1
2	$PDL_{13,\ TBD}$	60:0:1:1	30	rt	23.16	-	2.300	3,100	1.221	53.8
3	$PDL_{24,\ TBD}$	60:0:1:1	90	rt	39.06	-	3.900	5,000	1.099	75.2
4	$PDL_{36,TBD}$	60:0:1:1	120	rt	59.38	-	6,000	8,800	1.128	80.3
5	PF_{18}-*b*-$PDL_{13,\ TBD}$ [a]	0:18:1:1	10	-10	-	>99	8,500	14,300	1.393	68.3
6	PF_{18}-*b*-$PDL_{24,\ TBD}$ [a]	0:18:1:1	10	-10	-	>99	10,500	16,200	1.303	70.2
7	PF_{18}-*b*-$PDL_{36,\ TBD}$ [a]	0:18:1:1	10	-10	-	>99	12,500	20,000	1.353	63.1
8	PF_{18}-*b*-$PDL_{13,\ TBD}$	60:18:1:1	40	rt, -10	22.47	>99	7,400	14,600	1.233	67.5
9	PF_{18}-*b*-$PDL_{24,\ TBD}$	60:18:1:1	100	rt, -10	38.41	>99	10,100	16,300	1.252	66.8
10	PF_{18}-*b*-$PDL_{36,\ TBD}$	60:18:1:1	130	rt, -10	59.47	>99	12,800	18,500	1.311	65.3
11	PF_{55}-*b*-$PDL_{55,\ TBD}$	80:55:1:1	210	rt, -10	68.24	>99	26,880	28,700	1.503	63.2
12	PF_{18}-*b*-(PA-*alt*-EGE)$_{20,\ t\text{-BuP1}}$	20:20:18:1:0.5	100	100, -10	>99	>99	10,860	12,200	1.326	73.5
13	PF_{18}-*b*-(AA-*alt*-EGE)$_{20,\ t\text{-BuP1}}$	20:20:18:1:0.5	160	100, -10	>99	>99	10,600	14,800	1.351	52.3

[a]The reaction conducted after purification (dialysis) of the PDL. [b]Calculated by ^{1}H NMR spectroscopy of the polymers in $CDCl_3$. [c]Determined by SEC analysis in THF calibrated with polystyrene standards. (The ROP is conducted in bulk at 25°C, [TBD]:[4-iodobenzyl alcohol]:[δ-DL] = 1 : 1 : 60(80); SCTP is conducted in THF at -10°C, $[Pd_2(dba)_3]$:[*t*-Bu_3P]:[4-iodobenzyl alcohol]:[HexFL] = 0.4 : 2.2 : 1 : 18.

Table S2. The ROP of δ-DL catalyzed by TBD[a].

Run	Time (min)	Conv.[b] (%)	TOF (min^{-1})	$[M]_0/[M]_t$	$Ln\{[M]_0/[M]_t\}$	$M_{n,SEC}$[c] ($g\ mol^{-1}$)	$Đ$[c]
1	30	13.44	0.45	1.15	0.14	2,100	1.268
2	60	23.86	0.40	1.31	0.27	3,100	1.233
3	90	33.33	0.37	1.51	0.41	4,000	1.215
4	120	42.23	0.35	1.85	0.62	6,800	1.096
5	240	69.44	0.29	3.29	1.19	8,800	1.085
6	360	80.00	0.22	6.89	1.93	9,200	1.136

[a]The polymerization reactions are conducted in [TBD]:[4-Iodobenzyl alcohol]:[δ-DL] = 1 : 1 : 60 under 25°C. [b]The conversion of δ-DL is determined by ^{1}H NMR spectroscopy. [c]$M_{n,SEC}$ and $Đ$ are determined by SEC analysis in THF calibrated with polystyrene standards.

Table S3. Thermal properties of studied polymers.

Sample	T_d[a] (°C)	T_g[b] (°C)	T_m[c] (°C)	T_c[d] (°C)
PF_{18}	341.7	69.1	203.8	143.9
PDL_{36}	270.8	-55.2	--	--
PF_{18}-*b*-PDL_{13}	302.3	65.3, -58.7	176.7	130.4
PF_{18}-*b*-PDL_{24}	308.5	55.2, -57.3	172.9	122.3
PF_{18}-*b*-PDL_{36}	292.5	52.6, -53.9	166.7	124.5

[a]Degradation temperature at the heating/cooling rate of 10°C min^{-1} in thermogravimetric analysis (TGA) in a nitrogen atmosphere. [b]Midpoint temperature of glass transition at a heating rate of 10°C min^{-1} in differential scanning calorimetry (DSC) in a nitrogen atmosphere. [c]Melting temperature. [d]Crystallization temperature at a cooling rate of 10°C min^{-1} in differential scanning calorimetry (DSC) in a nitrogen atmosphere.

Table S4. Optical properties of studied polymers.

Sample	Solution [a]		As-cast film [d]		Annealed film [f]	
	λ_{max}^{abs} [b] (nm)	λ_{max}^{PL} [c] (nm)	λ_{max}^{PL} (nm)	PLQY [e] (%)	λ_{max}^{PL} (nm)	PLQY (%)
PF_{18}	383	420, 441	423, 445	24.33	423, 445	14.43
PDL_{36}	--	--	--	--	--	--
PF_{18}-*b*-PDL_{13}	383	420, 442	423, 448	32.28	423, 446	28.47
PF_{18}-*b*-PDL_{24}	383	420, 442	423, 448	35.16	423, 448	25.58
PF_{18}-*b*-PDL_{36}	383	420, 442	423, 447	37.29	423, 448	22.00

[a]In tetrahydrofuran. [b]Absorption at the longest wavelength. [c]Emission wavelength, excited at 365 nm. [d]The as-cast films of polymers were prepared on a glass substrate by spin-coating polymer solutions in tetrahydrofuran (1 mg mL^{-1}) at 3000 rpm. [e]Absolute PL quantum yield (PLQY) was recorded at excitation wavelength of 365 nm. [f]The films were annealed at 120 °C in vacuum for 1 day.

Table S5. The time-resolved PL spectra of PF_{18}-*b*-PDL_n thin films of as-cast state.

Sample	R^2 [a]	A_1 [b]	τ_1 [c]	τ_{avg} [d]
PF_{18}	0.9966	1.0994	0.1171	0.1171
PF_{18}-*b*-PDL_{13}	0.9972	1.0929	0.1372	0.1372
PF_{18}-*b*-PDL_{24}	0.9971	1.0608	0.1547	0.1547
PF_{18}-*b*-PDL_{36}	0.9965	1.1072	0.1692	0.1692

[a]Regression analysis constant of the fitting by a single exponential reconvolution of Figure 2d. [b]Number of photons at t = 0. [c]Time constant. [d]An average lifetime.